Probing Ligand Recognition in the Decarboxylase Antibody 21D8: Implications for the Catalytic Mechanism†

Kinya Hotta,‡,§ Ian A. Wilson,*,‡ and Donald Hilvert*,§

Department of Molecular Biology and Skaggs Institute for Chemical Biology, The Scripps Research Institute, 10550 North Torrey Pines Road, La Jolla, California 92037, and Laboratory of Organic Chemistry, Swiss Federal Institute of Technology, ETH-Hönggerberg, CH-8093 Zürich, Switzerland

Received September 28, 2001; Revised Manuscript Received November 14, 2001

ABSTRACT: Antibody 21D8, which was elicited with a naphthalene-1,5-disulfonate hapten, catalyzes the medium-sensitive decarboxylation of 5-nitro-3-carboxybenzisoxazole. Structural studies on the hapten−antibody complex show that the active site contains two anion binding pockets separated by a hydrophobic region. To gain further insight into the ligand binding and catalytic mechanism of 21D8, six site-directed mutants were prepared, four for investigating the role of each of the two hapten sulfonate binding sites and two for examining packing interactions between bound ligands and the binding pocket. With the exception of an $Arg^{L46}Met$ substitution in the more deeply buried sulfonate binding pocket, modification of the active site resulted in reductions in catalytic efficiency (k_{cat}/k_{uncat}), ranging between 3- and 23-fold. Importantly, and contrary to predictions based on computational docking experiments, the differential effects of the individual mutations on the K_m, K_{TS}, and $K_{product}$ parameters suggest that only substrate binding modes which place the carboxylate group in the more solvent-exposed sulfonate binding site are catalytically relevant. Such an orientation would permit a potentially significant interaction between the developing oxyanion in the transition state and the side chain of Arg^{L96}. Incomplete desolvation of the carboxylate in this orientation may also help explain the modest efficiency of 21D8 compared to the most accelerating aprotic dipolar organic solvents.

The rates of chemical transformations are often highly sensitive to the reaction medium. For example, many substitution and elimination reactions are accelerated more than 10^6-fold in organic solvents compared to the rates in water (*1*). Analogous medium effects are believed to contribute to the high efficiency of many enzymes (*2*). However, it is generally difficult to separate such effects from other contributions to the overall rate acceleration in these highly evolved, mechanistically complex systems.

The decarboxylation of 3-carboxybenzisoxazoles (i.e., **1** → **3**, Figure 1) is a typical solvent-sensitive transformation. Large rate increases are observed upon transfer of the reaction from an aqueous solution to aprotic dipolar solvents, such as hexamethylphosphoramide (*3*). This property has made the reaction a useful probe of microenvironmental effects provided by micelles (*4*), vesicles (*5*), synthetic polymers (*6*, *7*), and macrocyclic hosts (*8*). Antibody catalysts have also been developed to explore the contribution of medium effects in proteins (*9*−*11*).

Antibodies raised against the naphthalene-1,5-disulfonate derivative **4a** are particularly efficient catalysts for the decarboxylation of **1**, accelerating the reaction by as much as 23000-fold compared to the spontaneous reaction in water (*9*, *10*). Detailed kinetic analysis, heavy atom isotope effects, environmentally sensitive fluorescent probes, and computation (*9*, *10*, *12*, *13*) have been used to characterize one of the best decarboxylases, antibody 21D8. High-resolution structural studies of 21D8 with and without bound hapten have revealed an active site with two well-defined anion binding pockets separated by a hydrophobic region (Figure 2) (*14*). In conjunction with computational docking experiments (*14*), this structural information has provided valuable insight into how a mixture of polar and nonpolar sites might be exploited to bind the anionic substrate and accelerate a reaction normally facilitated by aprotic dipolar solvents.

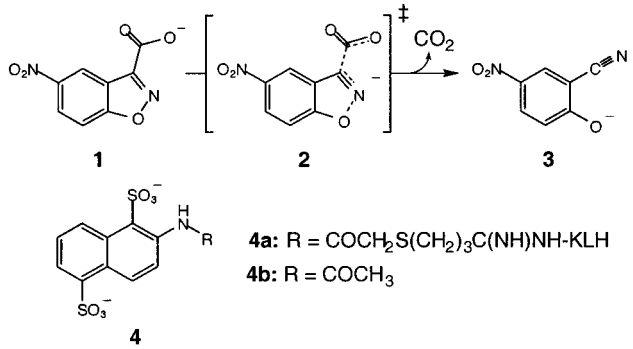

FIGURE 1: Decarboxylation of 5-nitro-3-carboxybenzisoxazole **1** proceeds through a charge-delocalized transition state **2** to give salicylonitrile **3** and carbon dioxide. The naphthalene-1,5-disulfonate derivative **4a** was used to elicit the decarboxylase antibody 21D8, whereas the acetamide **4b** was used for hapten inhibition assays.

† This work was supported in part by NIH Grants CA27489 (I.A.W.) and GM38273 (D.H. and I.A.W.) and the ETH Zürich and Novartis Pharma AG (D.H.).

* To whom correspondence should be addressed. I.A.W.: e-mail, wilson@scripps.edu; phone, (858) 784-9706; fax, (858) 784-2980. D.H.: e-mail, hilvert@org.chem.ethz.ch; phone, +41-1-632-3176; fax, +41-1-632-1486.

‡ The Scripps Research Institute.

§ Swiss Federal Institute of Technology.

10.1021/bi0158167 CCC: $22.00
Published on Web 12/27/2001

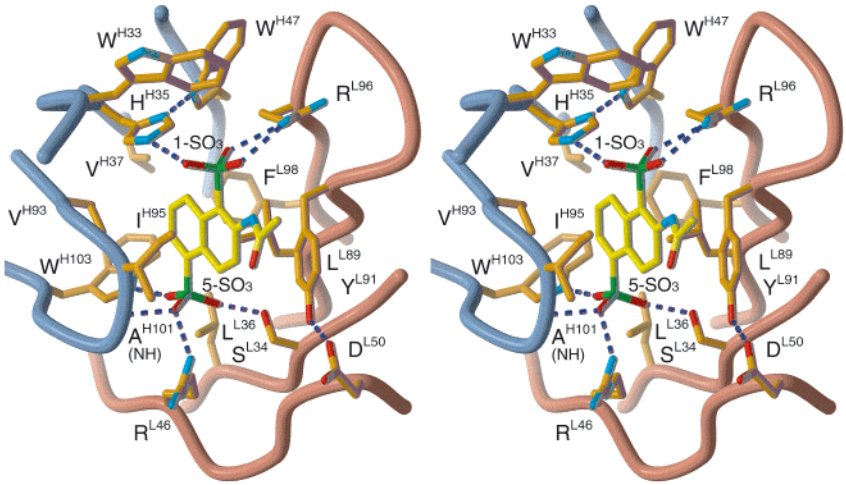

FIGURE 2: Stereoview of the 21D8 combining site with bound hapten. Cα traces of the light and the heavy chains are colored pink and blue, respectively. Side chains that contact the hapten are shown and numbered. Carbon atoms are yellow, oxygen atoms red, nitrogen atoms blue, and sulfur atoms green. This figure was created with programs Molscript (*42*), Raster3D (*43*), and Adobe Photoshop 5.0 (Adobe Systems Inc.). Reproduced with permission from *J. Mol. Biol.* (Academic Press).

Although hapten **4** fits into the 21D8 combining site in a unique orientation, the docking experiments predict that substrate **1** has several accessible binding modes (*14*). In the lowest-energy conformations, the benzisoxazole ring docks into the hydrophobic slot in such a way as to allow simultaneous binding of the 3-carboxylate at one of the anion binding sites and the 5-nitro group at the other. Specific hydrogen bonding interactions were also observed between Arg^{L46} and the developing oxyanion of the breaking N−O bond. The latter are potentially mechanistically significant, since theoretical studies have shown that such interactions can significantly lower the activation barrier for the decarboxylation reaction (*13*, *15*, *16*).

To test and refine these hypotheses, we have investigated 21D8 by site-directed mutagenesis. Here we describe the effects of mutating the two anion binding sites and residues lining the hydrophobic region of the binding pocket on catalytic efficiency as well as substrate, product, and hapten binding.

EXPERIMENTAL PROCEDURES

Materials. 5-Nitro-3-carboxybenzisoxazole **1**, 5-nitro-2-hydroxybenzonitrile **3a**, and 2-acetamidonaphthalene-1,5-disulfonate **4b** were synthesized according to published procedures (*3*, *9*) and gave satisfactory spectroscopic data. Restriction endonucleases and T4 DNA ligase were purchased from New England Biolabs or Fermentas. All PCRs[1] were performed with HotStarTaq DNA polymerase (Qiagen), using the provided reaction buffer. Oligonucleotides were custom-synthesized and purified by MicroSynth (Balgach, Switzerland). Media for experiments other than chimeric Fab production were prepared according to standard recipes (*17*). DNA sequencing was performed on an ABI 373 DNA sequencer (Perkin-Elmer Life Science) or an ABI PRIZM 310 genetic analyzer (PE Applied Biosystems). Mass spectra were obtained by electrospray ionization mass spectrometry (ESI-MS) on a Finnigan TSQ7000 Triple-Quad mass spectrometer.

Site-Directed Mutagenesis. Plasmid p4xH-21D8, which was previously constructed for expression of wild-type CF21D8 (*14*), served as the template for site-directed mutagenesis. Mutant codons were generally chosen to exploit the most frequently used codon for a particular amino acid among highly expressed genes in *Escherichia coli* (Wisconsin Sequence Analysis package, version 8, Genetics Computer Group, Inc.). Except for the $Leu^{L89}Phe$, $Arg^{L96}Leu$, Phe^{L98}-Leu, and $Val^{H93}Ile$ mutants, site-directed mutagenesis was accomplished by a standard overlap-extension PCR technique (*18*) using the following primers: 21D8 V_L flanking sense (5′-GCGGTTCAGAGCTCCAGCTGACTCAGTCT-3′, *Sac*I site underlined) and antisense (5′-TTTATTTCAAGCTTG-GTGCCTCCACCGAA-3′, *Hin*dIII site underlined), Ser^{L34}-Val mutagenic sense (5′-TGGTTACTTA**GTT**TGGCTT-CAGCAGAA-3′) and antisense (5′-TGCTGAAGCCA**AA**C-TAAGTAACCACTA-3′), $Arg^{L46}Met$ mutagenic sense (5′-CTATTAAAC**TG**CTGATCTACGACGCAA-3′) and antisense (5′-CGTCGTAGATCAG**CA**GTTTAATAGTTC-3′), 21D8 V_H flanking sense (5′-GTTAAGCTGGGGATCCTC-TAG-3′, *Bam*HI site underlined) and antisense (5′-GCA-GAGACGGTGACCAGAGTCCCTTG-3′, *Bst*EII site underlined), $Leu^{H5}Gln/Glu^{H6}Gln$ mutagenic sense (5′-TTCAGCT-GC**AGC**AGCCTGGGACTGA-3′) and antisense (5′-CC-AGGCT**GCT**GCAGCTGAACCTGAG-3′), $His^{H35}Ser$ mutagenic sense (5′-CCTACTGGATG**TCT**TGGGTGAAACA-3′) and antisense (5′-GTTTCACCCA**AGA**CATCCAGTAG-GA-3′), and $Val^{H37}Met$ mutagenic sense (5′-CACTGG**A**T-GAAACAGAGGCCTGGA-3′) and antisense (5′-GCCTCT-GTTTCA**T**CCAGTGCATCCAG-3′). For all primers, mutagenized positions are denoted in bold.

Because of the proximity of the site of mutation and the 3′-restriction site (*Hin*dIII for V_L and *Bst*EII for V_H), mutagenic antisense primers containing an appropriate restriction site were used in combination with the relevant flanking sense primer to introduce the $Leu^{L89}Phe$, $Arg^{L96}Leu$, and $Phe^{L98}Leu$ mutations in one PCR step. The antisense primers were as follows: 5′-GATCTCAAGCTTGGTGCCTCCAC-

[1] Abbreviations: CDR, complementarity determining region; CF, chimeric Fab; ELISA, enzyme-linked immunosorbent assay; IgG, gamma immunoglobulin; KLH, keyhde limpet hemocyanin; PCR, polymerase chain reaction; SDS−PAGE, sodium dodecyl sulfate−polyacrylamide gel electrophoresis; V_H domain, heavy chain variable domain; V_L domain, light chain variable domain.

CGAACGTCCGAGGAAAACTAGCATACTG**G**A-**A**ACAGTAATAGTCTG-3′ (*Hin*dIII site underlined) for Leu^{L89}Phe, 5′-GATCTCAAGCTTGGTGCCTCCACCGA-ACGTC**A**GAGGAAAACTAGCAT-3′ (*Hin*dIII site underlined) for Arg^{L96}Leu, and 5′-GATCTCAAGCTTGGTGC-CTCCACC**C**A**G**CGTCCGAGGAAAAC-3′ (*Bst*EII site underlined) for Phe^{L98}Leu.

Production, Purification, and Characterization of Chimeric Fab Fragments. The TOPP2 *E. coli* strain (Strategene) was transformed with p4xH-21D8 and its mutagenized derivatives for expression of the wild-type and mutant antibodies. High-density fermentation with the BIOFLO 3000 system (New Burnswick) was performed as previously described for production of all variants (*19*). The chimeric Fab fragment was purified from crude periplasmic lysates by protein G affinity chromatography, followed by Mono S cation-exchange chromatography. The purity of the sample was confirmed by SDS−PAGE. In some cases, isoelectric focusing gel electrophoresis and mass spectroscopic analysis were performed as further characterization of the mutant proteins. The final yield of the wild-type antibody was approximately 10 mg/L, while that of the mutants varied from <1 to ∼40 mg/L.

Kinetic and Binding Assays. All assays were performed in aqueous buffer [20 mM Tris-HCl and 50 mM NaCl (pH 8.0)] at 20 °C unless otherwise indicated. Initial rates for decarboxylation of **1** were determined spectroscopically by measuring the increase in absorbance at 380 nm ($\Delta\epsilon$ = 10 600 M^{-1} cm^{-1}) or 398 nm ($\Delta\epsilon$ = 3030 M^{-1} cm^{-1}). The data were corrected for the spontaneous background reaction, which was assessed under the same conditions and in good agreement with previously reported values (*3*). Steady state kinetic parameters k_{cat} and K_m were calculated from the initial rates using the Michaelis−Menten equation, $v_o/[E] = (k_{cat}[S])/(K_m + [S])$, where v_o is the initial rate, [E] is the antibody binding site concentration, and [S] is the substrate concentration.

Inhibition assays were carried out at a single substrate concentration (∼1.4 mM) in the presence of increasing amounts of hapten **4b**. The dissociation constant (K_{hapten}) of the hapten was determined by fitting the data to the equation:

$$v = [v_o/(2\alpha[E])][(K_{hapten} + [I] - \alpha[E])^2 + 4K_{hapten}\alpha[E] - (K_{hapten} + [I] - \alpha[E])]^{0.5}$$

where v is the initial rate in the presence of **4b**, v_o is the initial rate in the absence of hapten, α[E] is the fractional concentration of total antibody binding sites that are functional, and [I] is the inhibitor concentration (*20*).

Inhibition by product **3** was monitored similarly ([**1**] = 1.45 mM, [Fab] = 3.0 μM). Assuming that the product is a competitive inhibitor of the antibody, as is the case for the parent IgG (*9*), a linear relationship between $1/v$ and [P] is expected (*21*):

$$1/v = K_m[P]/(k_{cat}[E][S]K_{product}) + K_m/(k_{cat}[E][S]) + 1/(k_{cat}[E])$$

where v is the initial rate and E, S, and P are the antibody, substrate, and product, respectively. The dissociation constant for the product was determined from the slope of the resulting linear plot using independently determined k_{cat} and K_m values [$K_{product} = K_m/(k_{cat}[E][S]slope)$].

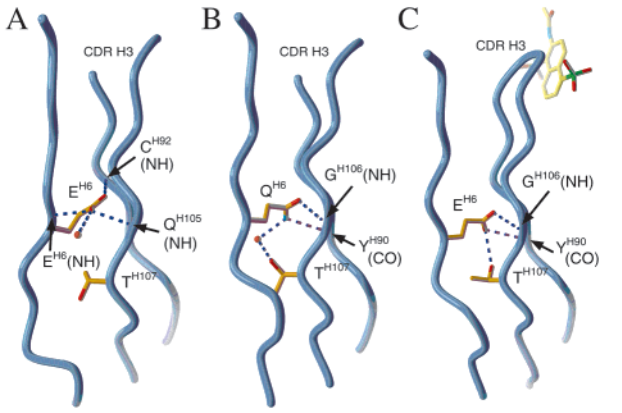

FIGURE 3: Representative interactions in the vicinity of residue H6 in typical antibodies. The coloring scheme is the same as in Figure 2. This site can be occupied by either a glutamate (A) or a glutamine (B). The structure of the same region in the chimeric 21D8 Fab fragment is shown (C) for comparison. Coordinates from the PDB were taken from entries 1A2Y (A), 1A6W (B), and 1C5C (C). This figure was created with programs Molscript (*42*), Raster3D (*43*), and Adobe Photoshop 5.0 (Adobe Systems Inc.).

RESULTS

Modification of the Binding Properties of Chimeric Fab 21D8. For structural studies, antibody 21D8 was originally expressed as a chimeric murine−human Fab fragment (*14*). This construct exhibited a somewhat higher acceleration rate than the parent IgG (k_{cat}/k_{uncat} = 61 000), but its affinity for hapten and substrate was approximately 20-fold lower. The high K_m of the chimera (∼5 mM) is particularly problematic for accurate kinetic analyses due to the limited solubility of substrate **1** in aqueous buffer [approximately 7 mM in 20 mM Tris-HCl and 50 mM NaCl (pH 8.0)]. For this reason, it was important to identify the origin of its altered affinity.

Although the human constant regions could conceivably perturb dimerization of the murine V_L and V_H domains, mutations introduced into the variable regions during cloning seemed more likely to be responsible for the altered properties of the chimera. These changes include the first, second, and last residues in the V_L domain and residues 5 and 6 in the V_H domain. Because the amino acids at the N- and C-termini of V_L are in structurally flexible regions, we initially focused on the H5 and H6 positions.

The side chain of H5 is relatively exposed to solvent, but that of H6 is buried within the interior of the V_H domain where it forms specific hydrogen bonds with the stem of the CDR H3 loop. During cloning, creation of an *Xho*I restriction site had converted the wild-type glutamines at positions H5 and H6 to a leucine and a glutamic acid, respectively. Although the sequence database shows that Gln and Glu occur with similar frequency at position H6 (*22*), comparison of known structures with these two residues at the H6 position reveals that the Gln and Glu side chains participate in distinct and highly conserved hydrogen bonding networks with surrounding residues (Figure 3A,B; see also Figure 5 of ref *23*). Because CDR H3 makes direct contacts with bound ligands in 21D8, and since it has been shown that loop conformations can be modified by distant mutations

Table 1: Kinetic Parameters and Inhibition Constants for 21D8 and Variants in Which the Bottom ($S^{L34}V$ and $R^{L46}M$) and Top ($R^{L96}L$ and $H^{H35}S$) Sulfonate Binding Sites Were Mutated[a,b]

	k_{cat} (s^{-1})	k_{cat}/K_m (s^{-1} M^{-1})	K_m (μM)	K_{TS} (μM)	$K_{product}$ (μM)	K_{hapten} (μM)
CF21D8	0.32	800	400	0.020	97	0.053
$S^{L34}V$	0.014	110	130	0.15	57	66
$R^{L46}M$	0.45	630	710	0.025	220	1.7
$R^{L96}L$	0.016	130	120	0.12	1600	0.22 ± 0.13
$H^{H35}S$	0.063	12 ± 2.3	5300 ± 840	1.3 ± 0.25	220 ± 45	0.51 ± 0.30

[a] Experiments were carried out in 20 mM Tris-HCl and 50 mM NaCl at pH 8.0 and 20 °C. [b] Unless otherwise indicated, standard errors are less than 15%.

(*24*), it seemed possible that changes at position H6 might influence ligand affinity (Figure 3C).

The expression plasmid p4xH-21D8, which provided good yields of the chimeric Fab (~10 mg/L of high-density cell culture) (*14*), was used as the template for mutagenesis. The gene for the $Leu^{H5}Gln/Glu^{H6}Gln$ double mutant, which restores the original amino acid sequence at the H5 and H6 positions, was constructed by standard overlap-extension PCR. The protein was produced in high yield (>20 mg/L) by fermentation. The purified protein, CF21D8, exhibits steady state parameters for the decarboxylation of **1** (k_{cat} = 0.32 s^{-1} and K_m = 400 μM) that are very similar to those of the wild-type IgG (k_{cat} = 0.28 s^{-1} and K_m = 210 μM). In addition, ELISA measurements and a kinetic titration assay with hapten analogue **4b** gave K_i values that were within a factor of 8 of the wild-type values (53 vs 6.8 nM).

The non-native sequence at positions H5 and H6 thus appears to account for most of the variation in ligand affinity between the chimeric 21D8 Fab and its parent IgG. The modest remaining difference in the K_m value for substrate **1** (2-fold) and the K_i value for hapten **4** (8-fold) can presumably be attributed to mutations at the N-terminus of V_L, which contacts the CDR L3 loop, another major hapten recognition element, and/or to small structural perturbations introduced by non-native interactions at the variable−constant domain interface and the hinge loops that connect the two domains. Nevertheless, the improved properties of the $Leu^{H5}Gln/Glu^{H6}Gln$ double mutant were sufficient for our purposes, and all additional mutations were introduced into this background.

Mutagenesis of the Bottom Sulfonate Binding Site. The regions of the 21D8 active site that mediate recognition of the haptenic 1- and 5-sulfonate groups are likely to be crucial for substrate binding and stabilization of the anionic transition state for decarboxylation (*14*). The recognition site for the 1-sulfonate group is relatively close to the mouth of the cavity, and we will refer to it as the top sulfonate site for simplicity (Figure 2). The 5-sulfonate recognition site is located deeper within the active site and will be termed the bottom sulfonate site. Both sites provide several hydrogen bond donors to the sulfonate oxygen atoms, and the positioning of the donor residues appears to be particularly suited for tetrahedral anion recognition. The side chains of residues Arg^{L96} and His^{H35} contribute to the top sulfonate site, while Ser^{L34}, Arg^{L46}, Trp^{H103}, and the backbone amide of Ala^{H101} comprise the bottom sulfonate site (Figure 2).

To investigate the role of the bottom sulfonate site, we targeted Ser^{L34} and Arg^{L46}, rather than the highly conserved Trp^{H103}, for replacement with nonpolar residues. Two single mutants, $Ser^{L34}Val$ and $Arg^{L46}Met$, were prepared. Valine was chosen to replace serine at position L34 on the basis of the crystallographic observation that the side chain of Ser^{L34} assumes a double conformation (*14*) that resembles the preferred conformation of a valine side chain. Whereas replacement of serine with an alanine would create a cavity corresponding to the serine Oγ atom, a valine residue was expected to fill the unoccupied space around L34. Valine occurs naturally at this position in other sequenced light chains, albeit rarely, at a frequency roughly 10% of that of serine (*22*).

Residue L46 is located at the V_L-V_H interface. Although leucine is the most commonly observed amino acid at this position (*22*), we worried that a β-branched residue might perturb the packing of the V_L and V_H domains. We consequently opted for methionine as the replacement for Arg^{L46}. Methionine occurs in only 0.11% of the known antibody sequences at this position (5 of 4522), but its extended side chain, like that of arginine, was expected to shield the pocket from bulk solvent.

The mutant genes were constructed using overlap-extension PCR and overexpressed in *E. coli* by fermentation. Sufficient amounts of Fab were obtained for thorough characterization of both variants. Steady state kinetic parameters, as well as binding constants for the product and hapten, were determined as previously described (*10*), and are summarized in Table 1.

The $Ser^{L34}Val$ mutation has a sizable deleterious effect on hapten binding and on the kinetic properties of 21D8. The modified sulfonate binding pocket poorly accommodates negatively charged species, as judged by the >1200-fold loss in hapten affinity. Moreover, the turnover number k_{cat} and the apparent second-order rate constant k_{cat}/K_m for the decarboxylation reaction decrease by 23- and 7.5-fold, respectively. Interestingly, the smaller Michaelis constant (K_m) observed for this mutant compared to that for the wild-type enzyme correlates with an increase in product affinity, suggesting that L34 interacts with a part of the substrate that does not change over the course of reaction. Binding of the nitrobenzene moiety of **1**, rather than the 3-carboxylate group, at the bottom sulfonate site would be consistent with this inference. While the hydrophobic valine side chain would be expected to destabilize the negatively charged sulfonate ion of the hapten, it should provide good packing interactions with the neutral nitrobenzene portion of the substrate and product, stabilizing their respective complexes with the antibody. The latter interactions probably also alter the orientation of the substrate within the binding site somewhat, placing the substrate carboxylate in an environment that is less favorable for decarboxylation. Because the affinity of the protein for the transition state as estimated by the relation $K_{TS} = k_{uncat}/(k_{cat}/K_m)$ (*25*) only decreases by 7.5-fold, the >20-fold drop in k_{cat} must reflect both ground and transition state effects.

Table 2: Comparison of Kinetic Parameters and Inhibition Constants for 21D8 and the Packing Mutants $L^{L89}F$ and $V^{H37}M$[a,b]

	k_{cat} (s^{-1})	k_{cat}/K_m (s^{-1} M^{-1})	K_m (μM)	K_{TS} (μM)	$K_{product}$ (μM)	K_{hapten} (μM)
CF21D8	0.32	800	400	0.020	97	0.053
$L^{L89}F$	0.017	100	170	0.16	770	0.49
$V^{H37}M$	0.092	27 ± 7	3500 ± 760	0.59 ± 0.15	67 ± 20	0.039 ± 0.031

[a] Experiments were carried out in 20 mM Tris-HCl and 50 mM NaCl at pH 8.0 and 20 °C. [b] Unless otherwise indicated, standard errors are less than 15%.

The effect of the $Arg^{L46}Met$ mutation is, in contrast, relatively modest. The change in hapten affinity is much smaller than that seen in the $Ser^{L34}Val$ mutant, suggesting that Arg^{L46} contributes comparatively little to the electrostatic stabilization of the hapten complex. Both the k_{cat} and K_m parameters for decarboxylation increase somewhat, resulting in virtually no change in the k_{cat}/K_m parameter and hence K_{TS}, compared to those of the parent antibody. On the basis of this kinetic profile, it is unlikely that Arg^{L46} provides a hydrogen bond or salt bridge to the developing oxyanion of the transition state, contrary to the predictions from docking experiments (*14*). However, the small, parallel increase seen in K_m and $K_{product}$ is consistent with the notion that the bottom sulfonate binding pocket is involved in recognition of the nitrobenzene unit, which the substrate and product have in common.

The importance of the 5-sulfonate and the acetamido groups for hapten recognition was further examined using analogues of **4**. For example, naphthalene-1-sulfonate binds to CF21D8 very weakly; a 20-fold molar excess of this compound over the substrate only inhibited the decarboxylase activity by approximately 67%. A similar extent of inhibition was observed with the two bottom-sulfonate-binding-site mutants, $Ser^{L34}Val$ and $Arg^{L46}Met$. These results suggest that both sulfonate binding sites must be occupied for ligands to bind to 21D8 with high affinity. In contrast, the acetamido group contributes relatively little to hapten affinity as judged by the fact that naphthalene-1,5-disulfonate binds to the parent antibody with a K_i of 420 nM, only ~5-fold lower than that for hapten **4**.

Mutagenesis of the Top Sulfonate Binding Site. The role of the top sulfonate site was probed by mutagenesis of residues L96 and H35. Arg^{L96} was replaced with a leucine on the basis of the fact that leucine is the most commonly observed residue at this position (*22*) and its side chain should reasonably fill the pocket generated by the removal of the arginine side chain. A serine was selected to replace His^{H35} in an attempt to preserve the highly conserved hydrogen bonding interaction with Trp^{H47}, which may be essential for the conformational integrity of the binding site CDR loops. Results obtained with the $Arg^{L96}Leu$ and $His^{H35}Ser$ variants are also presented in Table 1.

The $Arg^{L96}Leu$ mutant exhibits a 19-fold decrease in k_{cat} and a 6-fold decrease in k_{cat}/K_m compared to those of wild-type CF21D8. Unlike the $Ser^{L34}Val$ mutation, which causes similar changes in the steady state parameters, $Arg^{L96}Leu$ has a small effect on hapten binding (~4-fold increase in K_{hapten}) and a significantly larger effect on product affinity (~16-fold increase in $K_{product}$). The opposite effects on K_m and product affinity suggest that Arg^{L96} may interact with the portion of the substrate undergoing structural change during the reaction, namely, the carboxyisoxazole moiety. Such an interaction would allow simultaneous binding of the nitrobenzene portion of **1** at the bottom sulfonate site. Moreover, if the relative instability of the product complex resulted from loss of hydrogen bonding interactions between Arg^{L96} and the product phenolate oxygen, the 6-fold increase in K_{TS} could then be attributed to the loss of analogous stabilizing hydrogen bonding and/or electrostatic interactions between Arg^{L96} and the developing oxyanion in the transition state (*13*, *15*, *16*).

Replacement of His^{H35} with serine causes a 5-fold drop in k_{cat} and a 13-fold increase in the K_m value. Because all measurements were conducted at substrate concentrations below K_m, the error in the estimated kinetic parameters is large. Nonetheless, the $His^{H35}Ser$ variant exhibits the largest loss of catalytic efficiency (k_{cat}/K_m) among all the sulfonate binding site mutants (67-fold lower than that of CF21D8). Because His^{H35} is involved in a hydrogen bonding interaction with Trp^{H47}, which is a canonical feature of antigen binding pockets, it is possible that its replacement with a serine could cause significant changes in local active site geometry. The fact that the affinity of this mutant for hapten and product is not severely altered (approximately 10- and 2-fold decreases, respectively) argues against drastic structural changes in the binding pocket. Instead, significant destabilization of the bound ground state (to the extent that K_m reflects substrate affinity) and the even greater destabilization of the transition state upon removal of the imidazole ring is most consistent with a substantial perturbation in the immediate environment surrounding the substrate carboxylate.

Mutagenesis of the Hydrophobic Slot. The 1.7×10^4-fold rate acceleration achieved by 21D8 over the spontaneous reaction in water is still considerably smaller than the enhancements observed upon transfer of **1** to a number of aprotic dipolar solvents. However, hapten **4** is not an especially effective mimic of the transition state for decarboxylation (i.e., **2**), so it is not terribly surprising that antibodies that bind this compound are suboptimal for catalysis. There is presumably ample opportunity to improve on this first-generation decarboxylase.

One possibility that we considered was to restrict the freedom of the substrate within the binding pocket by replacing small hydrophobic residues that line the cavity with larger ones. Previous studies with a Diels−Alderase antibody have shown the benefit of such a strategy (*26*). Examination of the structure of the 21D8−hapten complex identified a cavity between the protein and ligand in the vicinity of residues H37 and L89. In an attempt to fill the extra space in the binding pocket and provide further binding interactions with the bound substrate, bulky residues were introduced at these positions. Two mutants, $Val^{H37}Met$ and $Leu^{L89}Phe$, were prepared and characterized (Table 2).

A small increase in hapten affinity was observed with $Val^{H37}Met$, but the $Leu^{L89}Phe$ mutation is unfavorable as

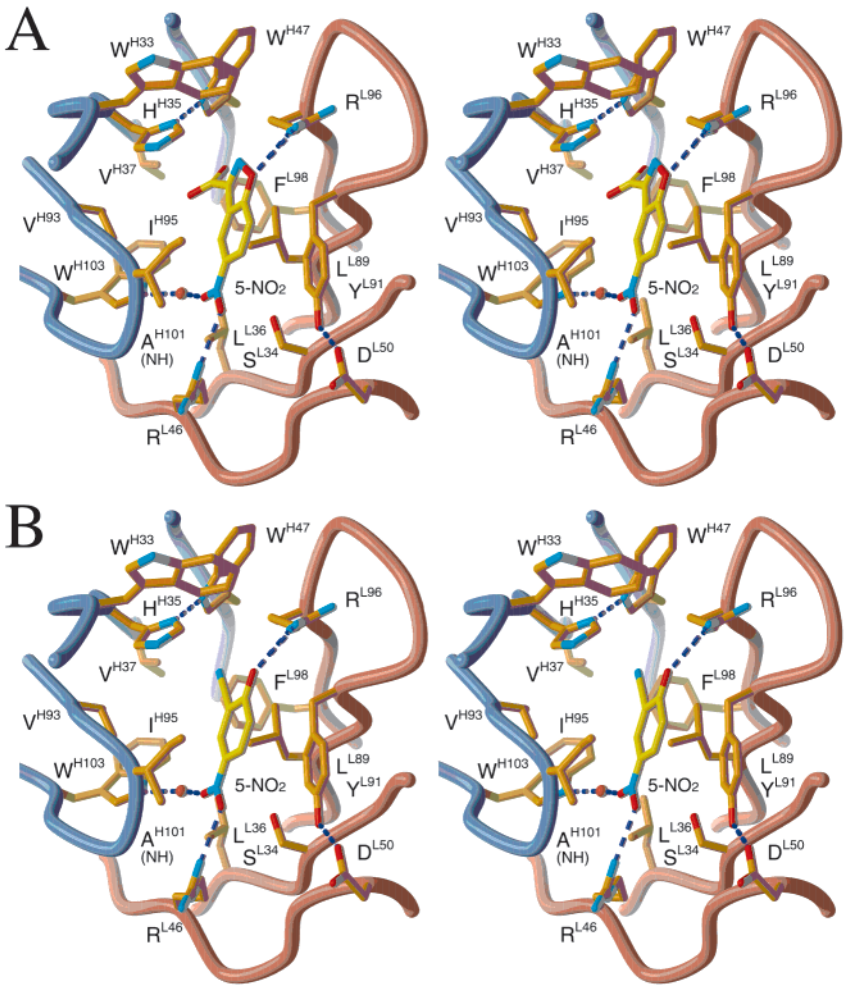

FIGURE 4: Models of 21D8−ligand interactions based on the hapten−21D8 complex structure and the results of mutagenesis experiments. The coloring scheme is the same as in Figure 2, and a water molecule is shown as a red sphere. Possible binding modes for the substrate and/or transition state (A) and product (B) that are consistent with the mutagenesis data are shown. This figure was created with programs Molscript (*42*), Raster3D (*43*), and Adobe Photoshop 5.0 (Adobe Systems Inc.).

judged by a 9-fold increase in K_{hapten}. More importantly, neither packing variant exhibits improved catalytic activity compared to CF21D8. Interestingly, they have opposite effects on K_m and $K_{product}$ that indicate different interactions with substrate and product for the two residues. Thus, the Val^{H37}Met mutation leads to an ~9-fold increase in K_m and a 1.4-fold decrease in $K_{product}$, whereas the Leu^{L89}Phe mutation gives an ~2-fold decrease in K_m and an ~8-fold increase in $K_{product}$.

DISCUSSION

Antibody 21D8 exhibits excellent shape and chemical complementarity to its hapten **4** (*14*). Mutagenesis of the 21D8 active site confirms that the two anion binding sites induced by the negatively charged sulfonate groups are important for hapten recognition. Modification of the bottom sulfonate site appears to destabilize the hapten complex more than mutation of the top sulfonate site (Table 1). Because insertion of a charged species into the low-dielectric environment of the protein interior is energetically very costly (*27*, *28*), loss of hydrogen bonding interactions in the buried pocket is presumably more detrimental than at the relatively solvent-exposed site. Attempts to improve shape complementarity in the complex by filling a small cavity between protein and ligand resulted in only a small increase in affinity for the hapten in the case of the Val^{H37}Met variant, but a significant decrease in affinity for Leu^{L89}Phe 21D8 (Table 2).

Earlier computational docking experiments (*14*) had suggested that both of the anion binding sites elicited by hapten **4** would also be important for the decarboxylase activity of 21D8. The docking experiments identified multiple plausible binding modes. In the lowest-energy orientations, the planar aromatic portion of **1** sits in the hydrophobic slot between the H3 and L3 CDR loops in such a way as to direct its carboxylate group into one of the sulfonate binding sites and the 5-nitro substituent into the other. Our mutagenesis results verify the importance of both sites in binding and catalysis, but the pattern and magnitude of the individual effects suggest that only the orientation in which the substrate carboxylate is in the top sulfonate site is catalytically relevant, as shown modeled into the active site (Figure 4A). Specifically, removal of potential hydrogen bond donors from the top site causes larger and generally deleterious changes in the K_m, K_{TS}, and $K_{product}$ parameters than does modification of the bottom binding pocket, consistent with a role in stabilizing the anionic species that occur across the reaction coordinate. Had the bottom sulfonate binding site been important for stabilizing these anions, we would have

expected much larger changes in the dissociation constants upon mutation of Ser^{L34} and Arg^{L46}, similar to the effects seen with the negatively charged hapten.

Stabilization of the incipient phenoxide in the transition state through hydrogen bonding interactions has been postulated to be a potentially important contributor to efficient catalysis of the decarboxylation reaction (*13*, *15*, *16*). However, the specific prediction that Arg^{L46} is the responsible residue in 21D8 (*14*) is not borne out by our results (Table 1). Instead, Arg^{L96} in the top sulfonate binding site appears to play this role. The parallel effects on K_{TS} and $K_{product}$ suggest that the positively charged guanidinium group sits close to the leaving group oxygen, where it can stabilize the (developing) negative charge electrostatically or by providing a hydrogen bond (Figure 4B). An arginine has been found at the same position in unrelated esterolytic antibodies generated in response to aryl phosphonates (*29*−*33*), and this residue is believed to serve an analogous role in stabilizing the tetrahedral anionic intermediate and transition states formed during ester hydrolysis. The effects of replacing Arg^{L96} with a nonpolar residue are significant, but not huge, probably because interactions with aqueous solvent can partially compensate for the missing interaction.

Binding of the substrate in an orientation that places its carboxylate group toward the mouth of the cavity may well help to explain the modest efficiency of 21D8 compared to the most accelerating aprotic dipolar solvents. Hydrogen bonding interactions with the carboxylate are known to strongly inhibit decarboxylation (*34*). Incomplete desolvation of the carboxylate when docked in the binding pocket would be expected to lead to significantly higher activation barriers for decarboxylation than for the same reaction in a purely aprotic dipolar medium. In this context, the significant destabilization of the transition state observed in the His^{H35}-Ser variant compared to the parent antibody may reflect an altered (less favorable) solvation environment for the carboxylate rather than a direct interaction between the carboxylate and the imidazole moiety. Ongoing efforts by Houk and his colleagues to develop a quantitative model for catalysis by 21D8 (personal communication) should help to enhance our understanding of this system.

With one exception (variant Arg^{L46}Met), substitution of residues that line the 21D8 binding site resulted in substantial decreases in catalytic efficiency (k_{cat}/k_{uncat}). This observation no doubt reflects the coarseness of the changes made and the subtle interplay of forces needed to gain high catalytic efficiency, but it also speaks to the challenge we face in trying to augment the activity of this first-generation catalyst by mutagenizing amino acids in direct contact with the bound ligand (*35*). An increasing number of studies on the affinity maturation of antibodies and the directed evolution of enzymes are showing that mutations far from the active site can contribute significantly to the optimization of binding and catalytic properties (*24*, *36*−*40*). Our own results with mutations at positions H5 and H6 in the 21D8 scaffold illustrate how seemingly minor structural adjustments can dramatically perturb interactions with a distant ligand. It is, therefore, likely that future efforts to improve this antibody will need to focus on residues in the second and third contact sphere beyond the active site. Although beneficial mutations of this type are difficult to predict from structural data alone, the convenient color change that accompanies the decarboxylation of **1** should facilitate the screening of large libraries of random variants.

The mutational analysis of 21D8 has provided valuable predictions regarding substrate binding and catalysis of the decarboxylation. In particular, the data presented here suggest that specific subsite interactions, rather than the general hydrophobic nature of the active site alone (*41*), directly influence catalytic efficiency. These results should prove to be useful in refining the computational model of this system (*14*), in analyzing the consequences of natural variation in families of related antibodies (*10*), and for guiding efforts to prepare more effective catalysts.

ACKNOWLEDGMENT

We thank H. D. Ulrich and P. G. Schultz for kindly providing expression plasmid p4xH-M13 and A. C. Backes for preparation of **1**.

REFERENCES

1. Reichardt, C. (1988) *Solvents and Solvent Effects in Organic Chemistry*, pp 121−283, VCH Verlagsgesellshaft mbH, Weinheim, Germany.
2. Jencks, W. P. (1975) *Adv. Enzymol. 43*, 219−410.
3. Kemp, D. S., and Paul, K. G. (1975) *J. Am. Chem. Soc. 97*, 7305−7312.
4. DiProfio, P., Germani, R., Savelli, G., Cerichelli, G., Spreti, N., and Bunton, C. A. (1996) *J. Chem. Soc., Perkin Trans. 2*, 1505−1509.
5. Scarpa, M. V., Araujo, P. S., Schreier, S., Sesso, A., Oliveira, A. G., Chaimovich, H., and Cuccovia, I. M. (2000) *Langmuir 16*, 993−999.
6. Shah, S. C., and Smid, J. (1978) *J. Am. Chem. Soc. 100*, 1426−1432.
7. Lee, J. J., and Ford, W. T. (1993) *J. Org. Chem. 58*, 4070−4077.
8. Schmidtchen, F. P. (1986) *J. Chem. Soc., Perkin Trans. 2*, 135−141.
9. Lewis, C., Krämer, T., Robinson, S., and Hilvert, D. (1991) *Science 253*, 1019−1022.
10. Tarasow, T. M., Lewis, C., and Hilvert, D. (1994) *J. Am. Chem. Soc. 116*, 7959−7963.
11. Hotta, K., Kikuchi, K., and Hilvert, D. (2000) *Helv. Chim. Acta 83*, 2183−2191.
12. Lewis, C., Paneth, P., O'Leary, M. H., and Hilvert, D. (1993) *J. Am. Chem. Soc. 115*, 1410−1413.
13. Zipse, H., Apaydin, G., and Houk, K. N. (1995) *J. Am. Chem. Soc. 117*, 8608−8617.
14. Hotta, K., Lange, H., Tantillo, D. J., Houk, K. N., Hilvert, D., and Wilson, L. A. (2000) *J. Mol. Biol. 302*, 1213−1225.
15. Gao, J. (1995) *J. Am. Chem. Soc. 117*, 8600−8607.
16. Na, J., Houk, K. N., and Hilvert, D. (1996) *J. Am. Chem. Soc. 118*, 6462−6471.
17. Sambrook, J., Fritsch, E. F., and Maniatis, T. (1989) *Molecular Cloning: A Laboratory Manual*, 2nd ed., Cold Spring Harbor Laboratory Press, Cold Spring Harbor, NY.
18. Aiyar, A., Xiang, Y., and Leis, J. (1996) *Methods Mol. Biol. 57*, 177−191.
19. Ulrich, H. D., Patten, P. A., Yang, P. L., Romesberg, F. E., and Schultz, P. G. (1995) *Proc. Natl. Acad. Sci. U.S.A. 92*, 11907−11911.
20. Williams, J. W., and Morrison, J. F. (1979) *Methods Enzymol. 63*, 437−467.
21. Todhunter, J. A. (1979) *Methods Enzymol. 63*, 383−411.
22. Kabat, E. A., Wu, T. T., Perry, H. M., Gottesman, K. S., and Foeller, C. (1991) *Sequences of Proteins of Immunological Interest*, 5th ed., National Institutes of Health, Bethesda, MD.
23. Honegger, A., and Plückthun, A. (2001) *J. Mol. Biol. 309*, 687−699.

24. Spiller, B., Gershenson, A., Arnold, F. H., and Stevens, R. C. (1999) *Proc. Natl. Acad. Sci. U.S.A. 96*, 12305−12310.
25. Wolfenden, R. (1969) *Nature 223*, 704−705.
26. Romesberg, F. E., and Schultz, P. G. (1999) *Bioorg. Med. Chem. Lett. 9*, 1741−1744.
27. Dao-Pin, S., Anderson, D. E., Baase, W. A., Dahlquist, F. W., and Matthews, B. W. (1991) *Biochemistry 30*, 11521−11529.
28. Baker, E. N., and Hubbard, R. E. (1984) *Prog. Biophys. Mol. Biol. 44*, 97−179.
29. Patten, P. A., Gray, N. S., Yang, P. L., Marks, C. B., Wedemayer, G. J., Boniface, J. J., Stevens, R. C., and Schultz, P. G. (1996) *Science 271*, 1086−1091.
30. MacBeath, G., and Hilvert, D. (1996) *Chem. Biol. 3*, 433−445.
31. Charbonnier, J. B., Golinelli-Pimpaneau, B., Gigant, B., Tawfik, D. S., Chap, R., Schindler, D. G., Kim, S. H., Green, B. S., Eshhar, Z., and Knossow, M. (1997) *Science 275*, 1140−1142.
32. Buchbinder, J. L., Stephenson, R. C., Scanlan, T. C., and Fletterick, R. J. (1998) *J. Mol. Biol. 282*, 1033−1041.
33. Tantillo, D. J., and Houk, K. N. (2001) *Chem. Biol. 8*, 535−545.
34. Kemp, D. S., Cox, D. D., and Paul, K. G. (1975) *J. Am. Chem. Soc. 97*, 7312−7318.
35. Bornscheuer, U. T., and Pohl, M. (2001) *Curr. Opin. Chem. Biol. 5*, 137−143.
36. Low, N. M., Holliger, P. H., and Winter, G. (1996) *J. Mol. Biol. 260*, 359−368.
37. Wedemayer, G. J., Patten, P. A., Wang, L. H., Schultz, P. G., and Stevens, R. C. (1997) *Science 276*, 1665−1669.
38. Arkin, M. R., and Wells, J. A. (1998) *J. Mol. Biol. 284*, 1083−1094.
39. Oue, S., Okamoto, A., Yano, T., and Kagamiyama, H. (1999) *J. Biol. Chem. 274*, 2344−2349.
40. Hoseki, J., Yano, T., Koyama, Y., Kuramitsu, S., and Kagamiyama, H. (1999) *J. Biochem. 126*, 951−956.
41. Hollfelder, F., Kirby, A. J., and Tawfik, D. S. (1996) *Nature 383*, 60−63.
42. Kraulis, P. J. (1991) *J. Appl. Crystallogr. 24*, 946−950.
43. Merritt, E. A., and Murphy, M. E. P. (1994) *Acta Crystallogr. D50*, 869−873.

BI0158167